

## RESEARCH ARTICLE

# Single-Crystal Polarized Raman Spectra of 6-Bromopyridine-2-carbaldehyde

Anna Luiza B. Brito<sup>1</sup>  | Bernardo A. Nogueira<sup>1,2</sup> | Gulce O. Ildiz<sup>3</sup> | Matteo Tommasini<sup>4</sup> | Rui Fausto<sup>1,3</sup> 

<sup>1</sup>CQC-IMS, Department of Chemistry, University of Coimbra, Coimbra, Portugal | <sup>2</sup>International Iberian Nanotechnology Laboratory (INL), Braga, Portugal | <sup>3</sup>Spectroscopy@IKU, Department of Physics, Faculty of Sciences and Letters, Istanbul Kultur University, Istanbul, Türkiye | <sup>4</sup>Dipartimento di Chimica, Materiali e Ingegneria Chimica “Giulio Natta”, Politecnico di Milano, Milan, Italy

**Correspondence:** Rui Fausto (rfausto@ci.uc.pt; r.fausto@iku.edu.tr)

**Received:** 29 April 2025 | **Revised:** 1 July 2025 | **Accepted:** 7 July 2025

**Funding:** This work was supported by the European Research Executive Agency (1011848998) and Fundação para a Ciência e a Tecnologia (UI0313B/QUI/2025, UI0313P/QUI/2025, LA/P/0056/2020).

**Keywords:** 6-bromopyridine-2-carbaldehyde | infrared spectrum | Raman polarized spectra | single crystal

## ABSTRACT

The room temperature (RT) single-crystal polarized Raman spectra of 6-bromopyridine-2-carbaldehyde (BPCA) have been obtained and interpreted based on fully periodic DFT calculations for the  $P2_1/a$  (No. 14; monoclinic) crystal of the compound. The calculations, performed with the CRYSTAL software employing the Becke three parameters Lee, Yang, and Parr (B3LYP) functional and the polarization-consistent triple-zeta valence plus polarization basis set (pob-TZVP), were able to reproduce very well the experimental data, thus allowing a detailed assignment of the Raman active  $A_g$  and  $B_g$  modes to individual bands. The isotropic non-polarized Raman spectrum of BPCA was also calculated and shown to agree very well with the corresponding experimental Raman spectrum. Finally, the RT infrared spectrum of BPCA was also revisited in light of the performed periodic calculations, improving on previously reported interpretation based on extrapolation of the interpretation of the spectra obtained for the isolated molecule of the compound to the crystalline phase. In this crystalline system, intermolecular interactions exert only a minor influence on the intramolecular vibrational potential. As such, this study also serves as a benchmark for the employed computational approach, demonstrating its ability to capture the effects of both crystallographic periodicity and symmetry on the polarization features of vibrational spectra.

## 1 | Introduction

We have recently reported on the structure, vibrational spectra, and photochemistry of 6-bromopyridine-2-carbaldehyde (BPCA) [1], which is a versatile building block in supramolecular chemistry and an important ligand in transition metal catalysts and luminescent complexes [2, 3]. Our previous investigation [1] included the study of the infrared (IR) spectra of the single molecule of the compound isolated in cryogenic Ar, Kr, and Xe matrices, and of the IR and depolarized Raman spectrum of polycrystalline powdered BPCA at room temperature (RT). In this article, we report on the RT single-crystal polarized Raman

spectra of BPCA. Single-crystal polarized Raman spectroscopy is an authoritative extension of traditional Raman spectroscopy, leveraging the polarization properties of light to extract additional insights into the vibrational characteristics of anisotropic materials, enabling precise determination of molecular orientations within anisotropic crystals, and providing a deeper understanding of their structural and dynamic properties [4–12].

The classical theory of Raman scattering describes the scattered light as originating from oscillating electric dipoles induced by the electric field of the incident light beam [13]. According to this model, the induced dipole moment vector,  $\mu'$ , is related to

the external electric field vector,  $\mathbf{E}$ , through the molecular polarizability tensor,  $\overline{\overline{\alpha}}$ . In its simplest form, neglecting non-linear terms, this relationship is expressed as follows:

$$\boldsymbol{\mu}' = \overline{\overline{\alpha}}\mathbf{E} \quad (1)$$

In the double harmonic approximation [13–16], for small displacements,

$$\alpha_{ij} \approx \alpha_{ij}^{(0)} + \sum_k \left( \frac{\partial \alpha_{ij}}{\partial Q_k} \right)_{Q_k=0} Q_k \quad (2)$$

where  $\alpha_{ij}^{(0)}$  is the  $i,j$ -component of the molecular polarizability at the equilibrium position, and  $\alpha'_{ij}{}^{(k)} = \left( \frac{\partial \alpha_{ij}}{\partial Q_k} \right)_{Q_k=0}$  is the component of the polarizability derivative tensor that represents how the polarizability changes due to molecular vibration  $Q_k$  taken at the equilibrium geometry.

The induced dipole component associated with the  $k$ -th Raman mode is then given by the following equation:

$$\boldsymbol{\mu}'^{(k)} = \overline{\overline{\alpha}}'^{(k)}\mathbf{E} Q_k \quad (3)$$

which can be explicitly written as follows:

$$\begin{bmatrix} \mu'_x \\ \mu'_y \\ \mu'_z \end{bmatrix}_k = \begin{bmatrix} \alpha'_{xx} & \alpha'_{xy} & \alpha'_{xz} \\ \alpha'_{yx} & \alpha'_{yy} & \alpha'_{yz} \\ \alpha'_{zx} & \alpha'_{zy} & \alpha'_{zz} \end{bmatrix}_k \begin{bmatrix} E_x \\ E_y \\ E_z \end{bmatrix} Q_k \quad (4)$$

Here, the coefficients  $\alpha'_{ij}$  correspond to the elements of the Raman polarizability tensor  $\overline{\overline{\alpha}}'^{(k)}$ , which contain the first derivatives of  $\overline{\overline{\alpha}}$  with respect to a Raman-active normal mode  $Q_k$ , evaluated at the molecule's equilibrium geometry. For non-resonant Raman scattering,  $\overline{\overline{\alpha}}'^{(k)}$  can be represented as a real, symmetric matrix, meaning  $\alpha'_{ij} = \alpha'_{ji}$ , reducing the number of independent components to a maximum of six.

In a crystalline material, the Raman polarizability tensor is typically referenced to the matter within the unit cell, and the contribution of the Raman polarizability tensor to the scattering intensity of the  $k$ -th normal mode is then given by the following equation:

$$\left| \mathbf{e}_i \overline{\overline{\alpha}}'^{(k)} \mathbf{e}_s \right|^2 \quad (5)$$

where  $\mathbf{e}_i$  and  $\mathbf{e}_s$  represent the polarization vectors of the incident and scattered photons, respectively [14–17]. The form of the Raman tensor  $\overline{\overline{\alpha}}'^{(k)}$  is determined by the symmetry of the vibrational mode. For a macroscopically oriented sample, the quantity  $\left| \mathbf{e}_i \overline{\overline{\alpha}}'^{(k)} \mathbf{e}_s \right|^2$  can become zero for specific photon polarization configurations. In such cases, the  $k$ -th vibrational mode is not Raman active for that particular scattering geometry. By analyzing the Raman tensor  $\overline{\overline{\alpha}}'^{(k)}$ , one can derive Raman selection rules for vibrational modes in different scattering configurations [17]. Conversely, by precisely controlling the polarization of both the incident and scattered photons, experimentally determined selection rules can be used to identify the symmetry of vibrational modes, thereby aiding in their assignment [17].

When analyzing anisotropic single crystals, the combination of the sample's orientation in the laboratory frame and the selected polarization directions of the incident and scattered light beams enables the determination of individual components of the Raman tensor through a series of complementary Raman experiments. However, extracting these components from experimental Raman intensity measurements is a challenging task. By analyzing the relative band intensities in carefully selected polarized Raman spectra, one can only obtain information on the relative values of the relevant polarizability components for different Raman-active modes. This limitation can be addressed through the combined use of experimental data and advanced computational methods. With the current accuracy of state-of-the-art computational approaches for predicting Raman activities, theoretical and experimental results can be leveraged synergistically. Additionally, by comparing computed Raman spectral patterns designed to replicate polarized light experiments against experimental data, one can assess the performance of the theoretical model in describing individual Raman tensor elements. This, in turn, provides a robust validation of the theoretically predicted Raman activities.

In the present study, we present a comprehensive analysis of the polarized Raman spectra of BPCA at RT, based on the detailed comparison of the experimental data with those resulting from state-of-the-art fully periodic electronic structure calculations following the linear combination of atomic orbitals (LCAO) approach as implemented in the CRYSTAL code [18], thus exploiting complementary experiments that probe the individual Raman tensor components. The RT IR spectrum of BPCA has also been revisited, taking into account the results of the present fully periodic calculations for the crystalline compound. In the studied crystalline system, intermolecular interactions are known to exert only a minor influence on the intramolecular vibrational potential [1]. As such, this study also serves as a benchmark for the employed computational approach, demonstrating its ability to capture the effects of both crystallographic periodicity and symmetry on the polarization features of vibrational spectra.

## 2 | Experimental and Computational Methods

A suitable crystal of commercially obtained BPCA, purity > 97%, was chosen for the Raman spectroscopic analysis. The Raman data were obtained at RT in a Raman Horiba LabRam HR Evolution system, with excitation at  $\lambda = 532$  nm (~50 mW at the sample; horizontally polarized). In order to change the polarization of the incident light by 90°, a half-wave polarization rotator (Horiba-Jobin-Yvon) was used, while a CorePol P-500-1000 polarizer (Horiba-Jobin-Yvon) was used to select the component of the scattered light to collect. The spot diameter of the laser was approximately 1  $\mu$ m and was focused on the sample surface through a 50 $\times$  long-working-distance objective (numerical aperture 0.5). The final spectra were the average of 50 accumulations of individual spectra collected during 10 s, with a spectral resolution of 0.5  $\text{cm}^{-1}$ . The calibration of the system was performed using as reference the silicon crystal Raman peak at 520.5  $\text{cm}^{-1}$ .

The IR spectrum of the compound was obtained in the attenuated total reflection (ATR) mode using a Thermo Scientific

FTIR Nicolet iS5 system, with an iD7 ATR accessory (angle of incidence: 45°; crystal: diamond). The spectrum was recorded with a spectral resolution of 2 cm<sup>-1</sup>, in the wavenumber range of 4000–400 cm<sup>-1</sup>, being the average of 64 scans.

BPCA crystallizes in space group P2<sub>1</sub>/a (No. 14; monoclinic), with  $a = 6.908(2) \text{ \AA}$ ,  $b = 6.290(4) \text{ \AA}$ ,  $c = 15.060(6) \text{ \AA}$ , and  $\beta = 95.57(3)^\circ$ , and four molecules per unit cell ( $Z = 4$ ) (CCDC 608389 [19]; Figure 1). The complete optimization of the BPCA crystal structure and the calculation of its Raman spectra were conducted using the CRYSTAL software [18], employing the Becke three-parameter Lee, Yang, and Parr (B3LYP) functional [20] and the polarization-consistent triple-zeta valence plus polarization basis set (pob-TZVP) [21]. Both atomic positions and the lattice parameters were optimized in all calculations. The initial structure used as input was that experimentally determined by Zhang et al. [19].

The CRYSTAL code has been previously used by our group to model properties of other crystalline systems [8, 11, 12] and presents relevant advantages for the simulating polarized Raman spectra. By using a Gaussian basis set within the LCAO framework to describe crystal orbitals, CRYSTAL simplifies the management of hybrid exchange–correlation functionals compared with plane-waves codes, allowing to more accurate predictions of vibrational spectra. Vibrational wavenumbers were obtained through the diagonalization of the dynamical matrix at the  $\Gamma$  point in the first Brillouin zone. The Cartesian force constants (i.e., the elements of the Hessian of the

potential energy, expressed in mass-weighted atomic Cartesian coordinates) were computed via numerical evaluation of the first derivatives of the analytical atomic gradients. CRYSTAL calculates Raman intensities accurately using the coupled perturbed Kohn–Sham (CPKS) method [18]. The Raman activity of the  $k$ -th normal mode,  $A_{ij}^{(k)}$ , corresponding to incident and scattered beams polarized in the  $i$  and  $j$  directions, respectively, is computed as  $A_{ij}^{(k)} = \left( \alpha_{ij}^{(k)} \right)^2$ , where  $\alpha_{ij}^{(k)}$  is the  $i, j$  component of the Raman tensor form mode  $k$ . For a static exciting field ( $\lambda_{\text{exc}} \rightarrow \infty$ ), the Raman intensities  $I_{ij}^{(k)}$  can then be calculated as  $I_{ij}^{(k)} = \frac{A_{ij}^{(k)}}{\omega_k}$ , with  $\omega_k$  representing the vibrational wavenumber of the normal mode  $k$ . By employing Gaussian basis set in the LCAO description of crystal orbitals, CRYSTAL allows efficient computation of Fock exchange, facilitating the use of hybrid functionals and enhancing the accuracy of vibrational spectra prediction [18, 22]. The wavenumbers computed at this level of theory showed indeed a better agreement with experimental data with respect to plane wave codes (employing local-density approximation or generalized gradient approximation functionals) in different cases [23–26].

### 3 | Results and Discussion

In the BPCA crystal, the molecules were found to be planar (the measured r.m.s. deviation from planarity for non-H atoms is 0.006(4) Å) [19]. They assume a conformation where the aldehyde oxygen atom points in the opposite direction of the nitrogen ring

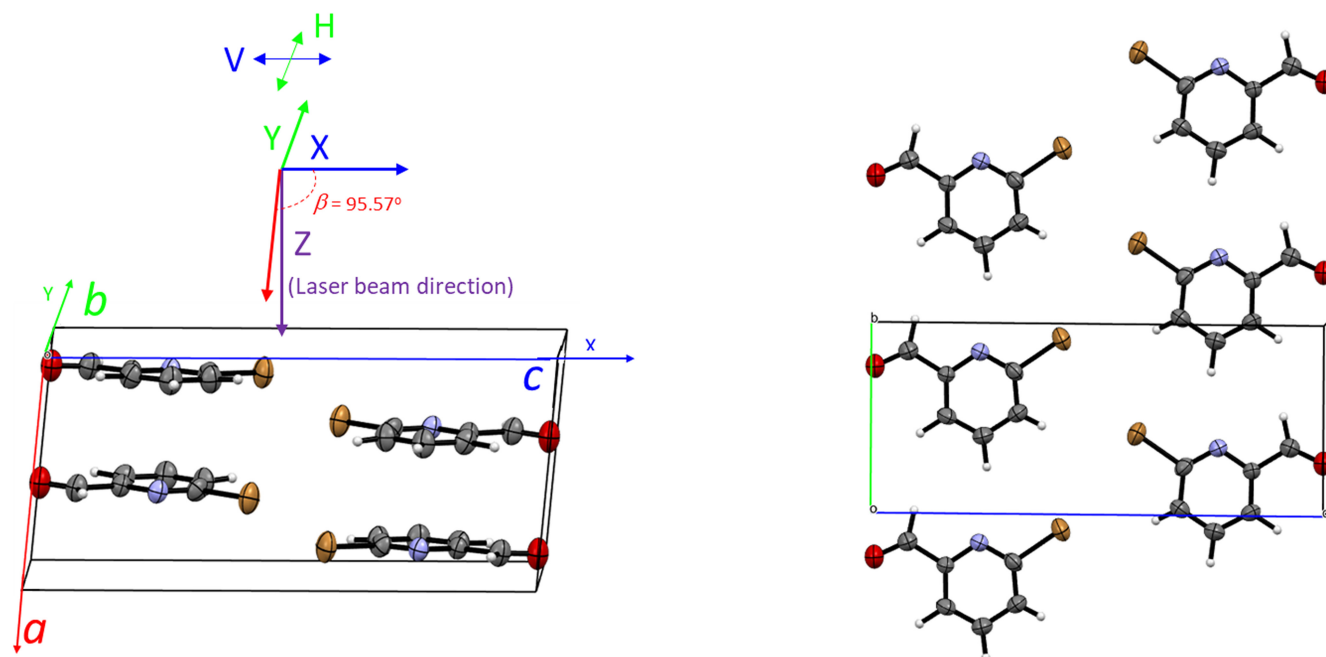


**FIGURE 1** | Unit cell representation of the P2<sub>1</sub>/a (No. 14; monoclinic) BPCA crystal, with indication of the reference frame ( $X, Y, Z$ ) and the directions of the laser beam ( $Z$ ) and polarization planes ( $X = H, Y = V$ ) (left), and view of the crystal arrangement viewed from the  $Z$  direction (right). According to the usual Porto's notation,  $A(BC)\bar{D}$ , where  $A$  and  $\bar{D}$  are the directions of propagation of incident and scattered light beam, and  $B$  and  $C$  are the polarization directions of the incident and scattered light, respectively, the geometry shown in the figure allows to collect the  $Z(XX)\bar{Z}$ ,  $Z(XY)\bar{Z}$ ,  $Z(YX)\bar{Z}$ , and  $Z(YY)\bar{Z}$  spectra (with  $X$  and  $Y$  coinciding with the directions of the  $c$  and  $b$  crystallographic axes), which correspond to the vertical–vertical (VV), vertical–horizontal (VH), horizontal–vertical (HV), and horizontal–horizontal (HH) experimental geometries, respectively. In this work, the  $Y(XX)\bar{Y}$ ,  $Y(XZ)\bar{Y}$ ,  $Y(ZX)\bar{Y}$ , and  $Y(ZZ)\bar{Y}$  spectra and the  $X(ZZ)\bar{X}$ ,  $X(ZY)\bar{X}$ ,  $X(YZ)\bar{X}$ , and  $X(YY)\bar{X}$  spectra were also measured by changing the relative orientation of the crystal and laser beam direction.

atom (*trans* conformer [1, 19]; see Figure 1). The BPCA molecules are linked into chains along the direction of the crystallographic *b* axis by weak intermolecular C–H⋯N hydrogen-bond-like interactions ( $d_{\text{H}\cdots\text{N}} = 2.53(6) \text{ \AA}$ ;  $d_{\text{C}\cdots\text{N}} = 3.534(7) \text{ \AA}$ ;  $\angle_{\text{C-H}\cdots\text{N}} = 167(4)^\circ$ ) and form columns along the *a* axis direction, where the molecules are symmetry related by a  $2_1$  screw-axis symmetry transformation, so that in adjacent layers they are rotated by  $\sim 180^\circ$  in relation to each other while the nitrogen atom of a given molecule stays nearly above the center of the rings of the neighboring molecules. There are 4 molecules per unit cell ( $Z=4$ ), with the asymmetric unit containing 1 molecule ( $Z'=1$ ). Thus, assuming the  $C_s$  symmetry for the molecules in the crystal, the 33 vibrations of the isolated molecule (23  $A'$  and 10  $A''$ ) will give rise to  $4 \times (33 + 6) = 156$  modes, with 132 being internal vibrations and 24 external modes, the latter including the 3 acoustic modes and 21 optical modes.

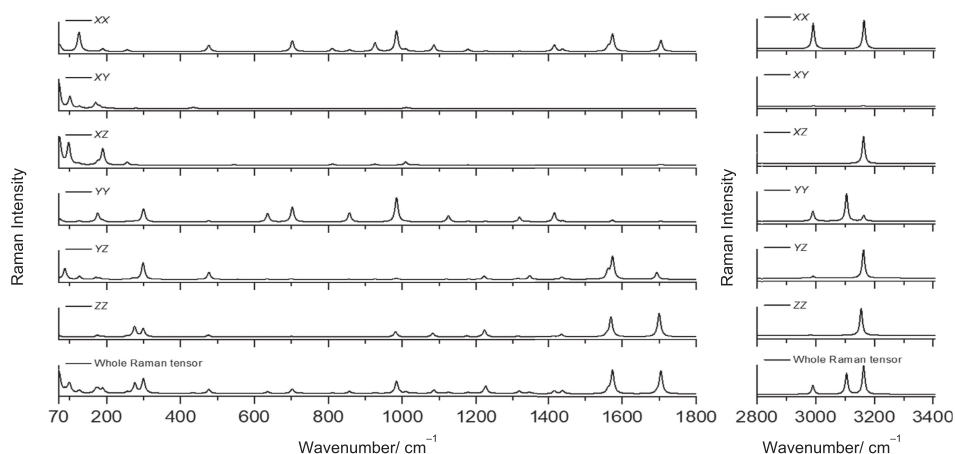
In the space group  $P2_1/a$  (No. 14), with  $Z=4$  and  $Z'=1$ , the BPCA molecules occupy general positions with site symmetry  $C_1$ . The factor group is  $C_{2h}$ , so that the vibrations span the irreducible representations  $39 A_g + 39 A_u + 39 B_u + 39 B_g$ . The  $4 \times 33 = 132$  internal vibrations in the crystal are equally divided by the 4 symmetry species, i.e.,  $33 A_g + 33 A_u + 33 B_g + 33 B_u$ , from which the  $A_g$  and  $B_g$  modes are Raman active and the  $A_u$  and  $B_u$  are IR active. External acoustic modes are of  $A_u + 2 B_u$  symmetry, and external optical modes are  $6 A_g + 5 A_u + 6 B_g + 4 B_u$ . This means that, the symmetry selection rules predict that  $39 (A_g) + 39 (B_g) = 78$  fundamental vibrations can be expected to contribute to the Raman spectrum of crystalline BPCA, while  $38 (A_u) + 37 (B_u) = 75$  vibrations are infrared active.

In the Raman experiments, the selected crystal of the compound was mounted on the microscope stage, with the different faces perpendicular to the laser beam, as illustrated in Figure 1, the scattered light being collected using the backscattering geometry. By choosing the reference Cartesian  $XYZ$  system in such a way that  $Z$  is aligned along the laser beam and  $X$  and  $Y$  are the directions of the *c* and *b* crystallographic axis, respectively, as shown in Figure 1, the four distinct Raman spectra collected can be described using the Porto notation as  $Z(XX)\bar{Z}$ ,  $Z(XY)\bar{Z}$ ,

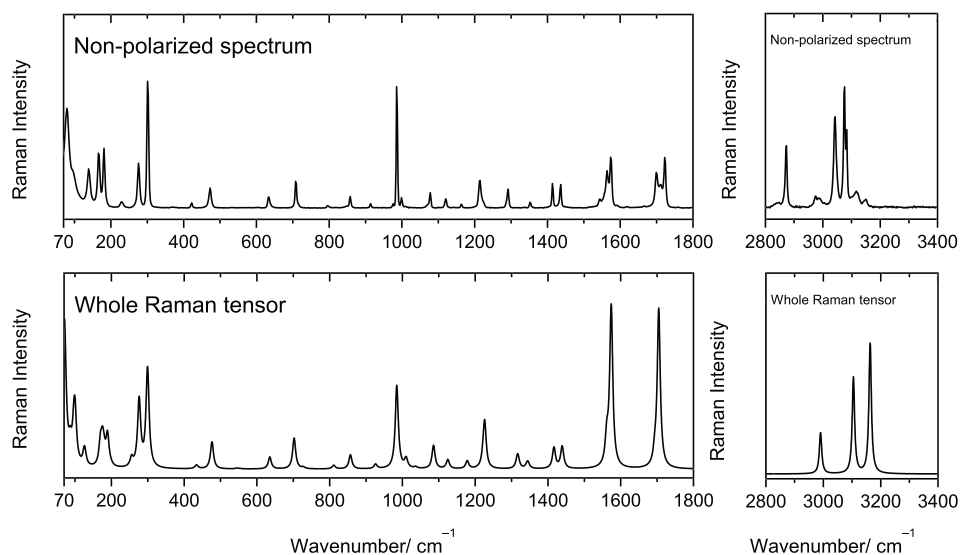
$Z(YX)\bar{Z}$ , and  $Z(YY)\bar{Z}$ , which highlight the different incident/scattered light polarization directions, respectively: vertical–vertical (VV), vertical–horizontal (VH), horizontal–vertical (HV), and horizontal–horizontal (HH). Changing the relative orientation of the crystal faces and laser beam direction, the remaining polarized spectra could also be measured.

Figure 2 present the B3LYP/pob-TZVP calculated spectra of the BPCA  $P2_1/a$  crystal using CRYSTAL, showing the calculated unpolarized spectrum obtained using the whole Raman tensor and those built using the individual tensor components (abbreviated in the figure by the corresponding Cartesian indexes). All spectra are normalized to their highest-intensity peak. The non-polarized Raman spectrum of the BPCA crystal and the different experimental polarized Raman spectra (VV, VH, HV, and HH, for the three alternative face orientations of the crystal relative to the laser beam direction used) are shown in Figures 3–6, together with the calculated spectra built based on the relevant components of the Raman tensors. For all three orientations examined, the spectra where the incident and scattered light were obtained with the same polarization (either VV and HH, or, in the Porto notation, e.g.,  $Z(XX)\bar{Z}$  and  $Z(YY)\bar{Z}$ , respectively; see Figure 1) show significant differences, while, as expected, the spectra obtained with orthogonal polarizations (VH and HV, or, e.g.,  $Z(XY)\bar{Z}$  and  $Z(YX)\bar{Z}$ ) are practically superimposable and distinct from the previous ones. As seen in the figures, the relevant calculated polarized Raman spectra show excellent agreement with the experimental data. The assignments of both unpolarized and polarized Raman spectra are provided in Table 1.  $A_g$  symmetry modes are observed exclusively for all VV and HH combinations and also in the case of the VH/HV spectra corresponding to Porto notations  $Y(XZ)\bar{Y}$  and  $Y(ZX)\bar{Y}$ , while the  $B_g$  modes are observed alone in both the  $Z(XY)\bar{Z}/Z(YX)\bar{Z}$  and  $X(\bar{Y}Z)\bar{X}/X(\bar{Z}Y)\bar{X}$  pairs of spectra.

Considering the excellent reproduction of the experimental spectra by the calculated ones, assignments were made straightforwardly. In Table 1, the designations of the modes follow those in ref. [1]. The Table presents the calculated Raman wavenumbers (unscaled and scaled), the calculated activities associated with the different Raman tensor components and for the isotropic



**FIGURE 2** | B3LYP/pob-TZVP calculated spectra of the BPCA  $P2_1/a$  crystal using CRYSTAL. The figure shows the calculated unpolarized spectrum, obtained with the full Raman tensor, and those obtained using the individual tensor components (abbreviated in the figure with Cartesian indexes). All spectra are normalized to their highest-intensity peak in each shown spectral region. Wavenumbers were scaled by the factor 0.9875, which was determined by fitting the calculated to experimental frequencies (most intense bands).



**FIGURE 3** | Experimental non-polarized Raman spectrum of the BPCA  $P2_1/a$  crystal compared with the B3LYP/pob-TZVP calculated spectrum based on the whole crystal Raman tensor. Calculated wavenumbers were scaled by 0.9875.

unpolarized spectrum, as well as the corresponding calculated intensities. The experimentally observed wavenumbers are also shown in the Table, together with the approximate descriptions of the vibrations (complete zipped file of the calculated eigenvectors are available from the authors upon request). For both isotropic unpolarized spectra, the identical intramolecular modes of  $A_g$  and  $B_g$  symmetry are assigned to the same band, due to the associated small Davydov splitting (factor group splitting), in line with the conclusions extracted in our previous investigation that the intermolecular interactions in the BPCA crystal do not perturb significantly the intramolecular vibrational potential [1]. The exception to this is the two modes associated with the torsion around the exocyclic C–C bond ( $\tau$ C–C), which are observed as separate bands in the isotropic unpolarized Raman spectrum, at  $167\text{ cm}^{-1}$  ( $B_g$ ) and  $138\text{ cm}^{-1}$  ( $A_g$ ), and are predicted at  $170$  and  $125\text{ cm}^{-1}$ , respectively. In the polarized spectra, on the other hand, due to the fact that  $A_g$  and  $B_g$  modes are exclusively observed in different spectra, all modes could be assigned individually (see Figures 4–6 and Table 1).

In the high wavenumbers range, the experimental isotropic unpolarized Raman spectrum shows satellite bands at  $3150$ ,  $3118$ ,  $2988$ ,  $2975$  and  $2842\text{ cm}^{-1}$  (Figure 3). In the polarized Raman spectra, these bands are prominent only in the  $X(YY)\bar{X}$  and  $Z(YY)\bar{Z}$  spectra, and must then be assigned to overtones or combination tones of  $A_g$  symmetry which may be experiencing some degree of intensification by Fermi resonance with the  $\nu$ C–H  $A_g$  fundamentals. Tentative assignments for the non-fundamental bands in this spectral region are:  $2 \times 1575$  ( $\nu$ ring1  $B_g$ ) =  $3150\text{ cm}^{-1}$ ,  $1702$  ( $\nu$ C=O  $A_g$ ) +  $1416$  ( $\nu$ ring5/ $\delta$ CH3  $A_g$ ) =  $3118\text{ cm}^{-1}$ ,  $1567$  ( $\nu$ ring2  $A_g$ ) +  $1416$  ( $\nu$ ring5/ $\delta$ CH3  $A_g$ ) =  $2983\text{ cm}^{-1}$ ,  $1565$  ( $\nu$ ring2  $B_g$ ) +  $1410$  ( $\nu$ ring5/ $\delta$ CH3  $A_g$ ; non-observed) =  $2975\text{ cm}^{-1}$ , and  $1724$  ( $\nu$ C=O  $A_g$ ) +  $1216$  ( $\delta$ CH1/ $\nu$ C–C  $A_g$ ) =  $2940\text{ cm}^{-1}$ . In the low wavenumbers range (below  $1800\text{ cm}^{-1}$ ) the reproduction of the isotropic non-polarized Raman spectrum by the calculations is excellent, and only the band splitting observed for the  $\nu$ C=O ( $1722/1711/1702\text{ cm}^{-1}$ ) and  $\nu$ ring1 ( $1574/1563\text{ cm}^{-1}$ ) modes shall be commented. The splitting of the  $\nu$ C=O band is also observed in the polarized Raman spectra for both the  $A_g$  and  $B_g$   $\nu$ C=O modes and can be ascribed to

Fermi resonances with the overtones of the  $A_g$  and  $B_g$  fundamental modes observed at  $859$  and  $858\text{ cm}^{-1}$  in the polarized spectra (at  $858\text{ cm}^{-1}$  as a single band in the isotropic unpolarized spectrum) in the case of the  $\nu$ C=O  $A_g$  mode, and to Fermi resonance with the combination of these two modes in the case of the  $\nu$ C=O  $B_g$  mode. In turn, the splitting observed in the  $\nu$ ring1 band in the non-polarized spectrum is most probably also due to a Fermi resonance interaction, this time with the overtone of the  $\gamma$ CH1  $A_g$  mode, observed at  $805\text{ cm}^{-1}$  in the polarized Raman spectra (and at  $795\text{ cm}^{-1}$  in the isotropic unpolarized spectrum). It is also interesting to note that the band splitting observed in these two modes accounts also for the apparent low intensity of their bands in the experimental spectra compared with the calculated spectra when peak intensity is considered instead of the integrated intensity (see Figures 2–6). The opposite effect can be noticed in the peak intensity vs. integrated intensity of the bands due to the  $\delta$ ring1 mode at  $\sim 990\text{ cm}^{-1}$ , which is the narrowest band in the spectra, leading to its apparent larger intensity compared with the remaining bands when peak intensities are observed.

In addition to the detailed investigation of the Raman spectra of BPCA, in the present work, we also revisited its RT IR spectrum in light of the performed fully-periodic calculations. In our previous work [1], we have used the calculated spectrum for the isolated molecule of the compound to help interpret the experimental data, based on our conclusion that the intermolecular interactions in crystalline BPCA are not strong and perturb only marginally the intramolecular vibrational potential [1]. The results now obtained are shown in Figure 7 and Table 2. The band assignments follow closely those previously done, confirming the reduced coupling between intra- and intermolecular modes.

Nevertheless, the present calculations suggest a different description of the  $\nu$ C–H vibrations compared with the isolated molecule. In the crystal, the three modes are essentially localized in a single C–H bond (as indicated in Tables 1 and 2), while in the isolated molecule, the stretching modes of the C(3)–H and C(5)–H bonds combine with each other [1]. The uncoupling of the  $\nu$ C–H vibrations in the crystal can be correlated with the

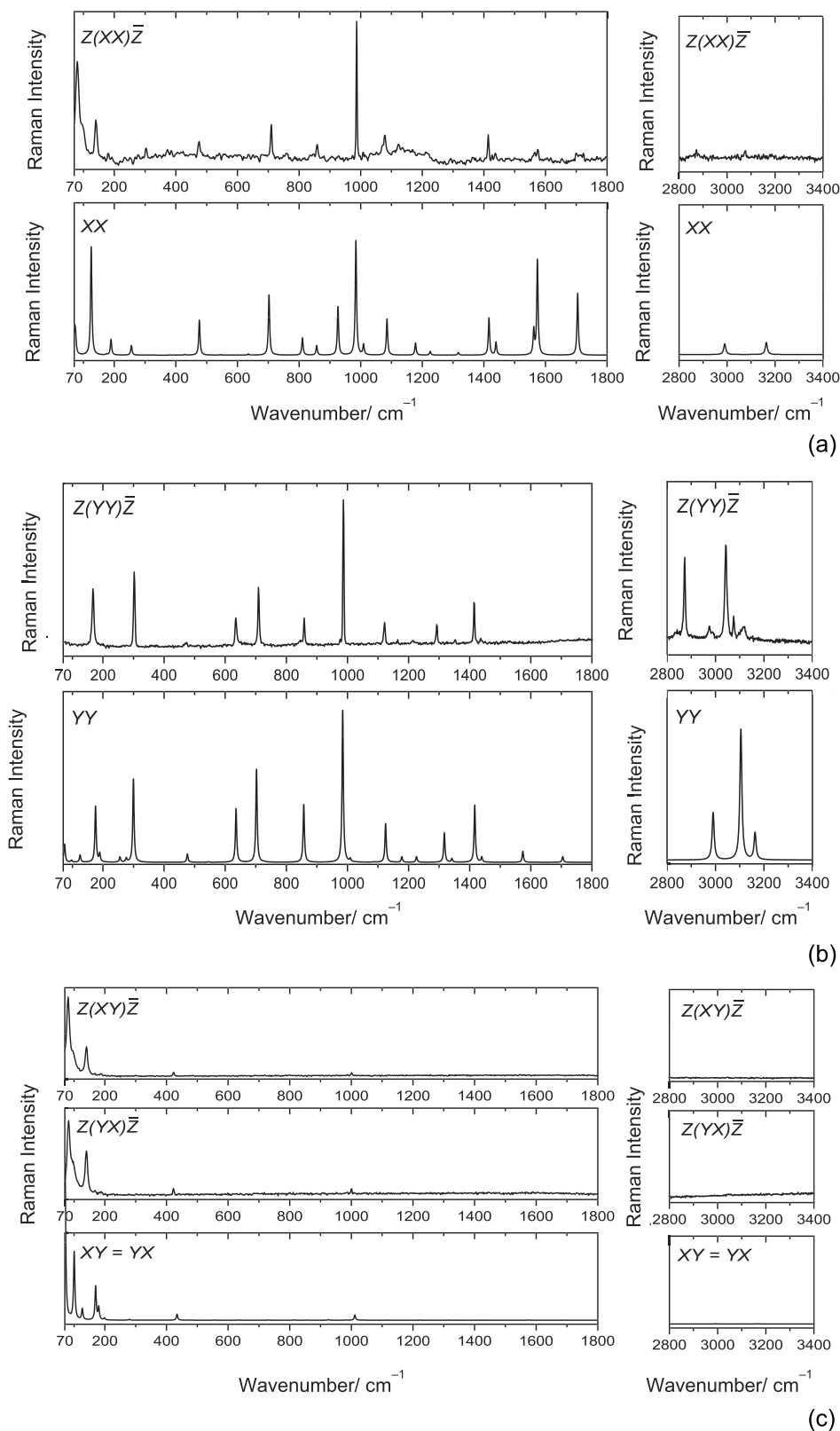


**FIGURE 4** | Experimental polarized  $Z(XX)\bar{Z}$  (VV),  $Z(YY)\bar{Z}$  (HH),  $Z(XY)\bar{Z}$  (VH), and  $Z(YX)\bar{Z}$  (HV) Raman spectra ( $X$  and  $Y$  are aligned with  $b$  and  $c$  crystallographic axes, respectively) of the BPCA  $P2_1/a$  crystal compared with the B3LYP/pob-TZVP calculated spectra based on the  $XX$ ,  $YY$ , and  $XY=YX$  component of the crystal Raman tensor. Calculated wavenumbers were scaled by 0.9875.

different intermolecular environment. The C(3)-H bond is located close to the aldehyde oxygen atoms of the two neighboring molecules staying in the layers immediately above and below

along the  $a$  direction, thus experiencing attractive-type intermolecular interactions, while the C(5)-H bond is not involved in any short contact [19]. Also, the present calculations suggest

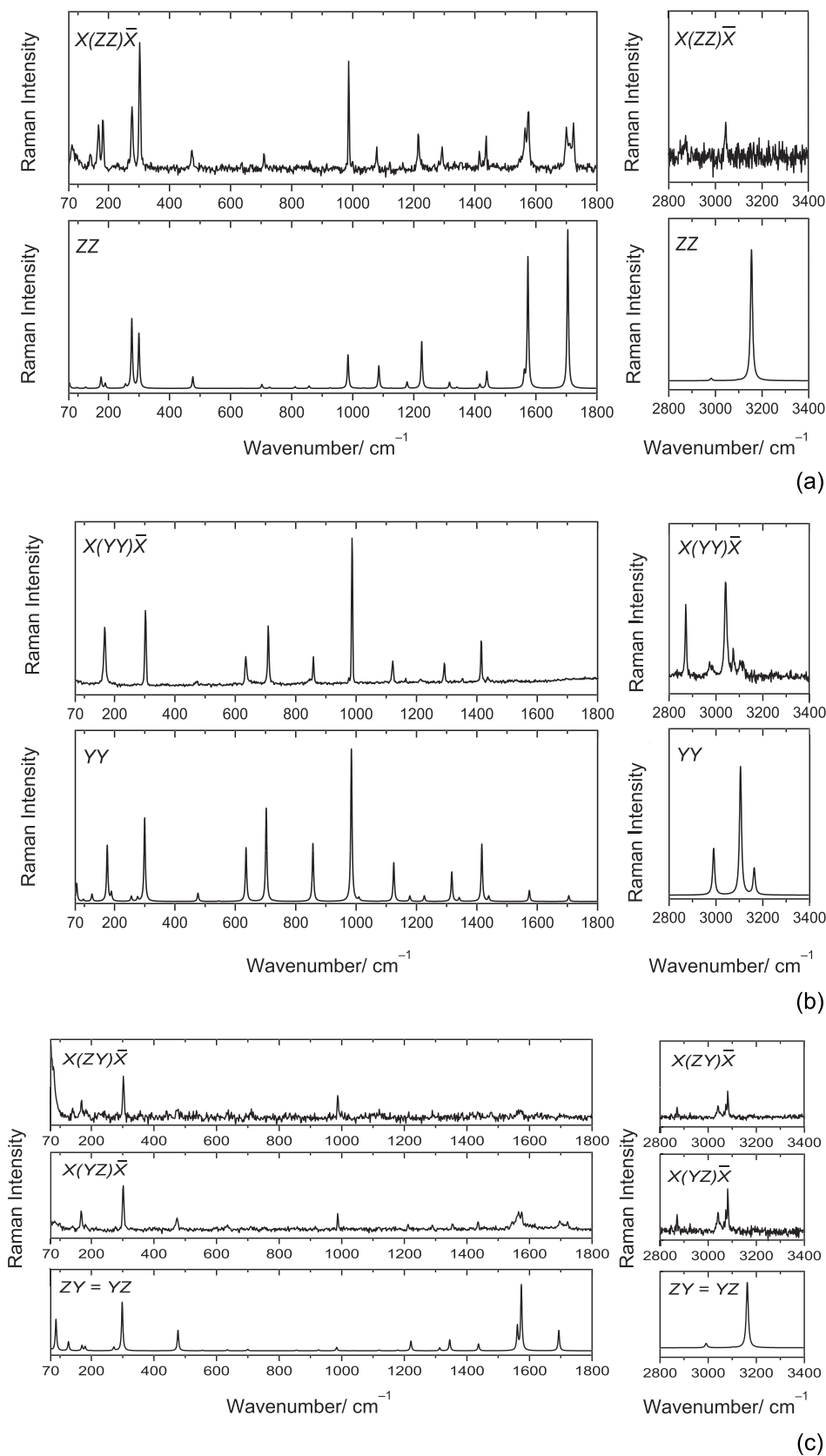


**FIGURE 5** | Experimental polarized  $X(ZZ)\bar{X}$  (VV),  $X(YY)\bar{X}$  (HH),  $X(ZY)\bar{X}$  (VH), and  $X(YZ)\bar{X}$  (HV) Raman spectra (Z and Y are aligned with  $a$  and  $c$  crystallographic axes, respectively) of the BPCA  $P2_1/a$  crystal compared with the B3LYP/pob-TZVP calculated spectra based on the  $YY$ ,  $ZZ$ , and  $YZ = ZY$  component of the crystal Raman tensor. Calculated wavenumbers were scaled by 0.9875.

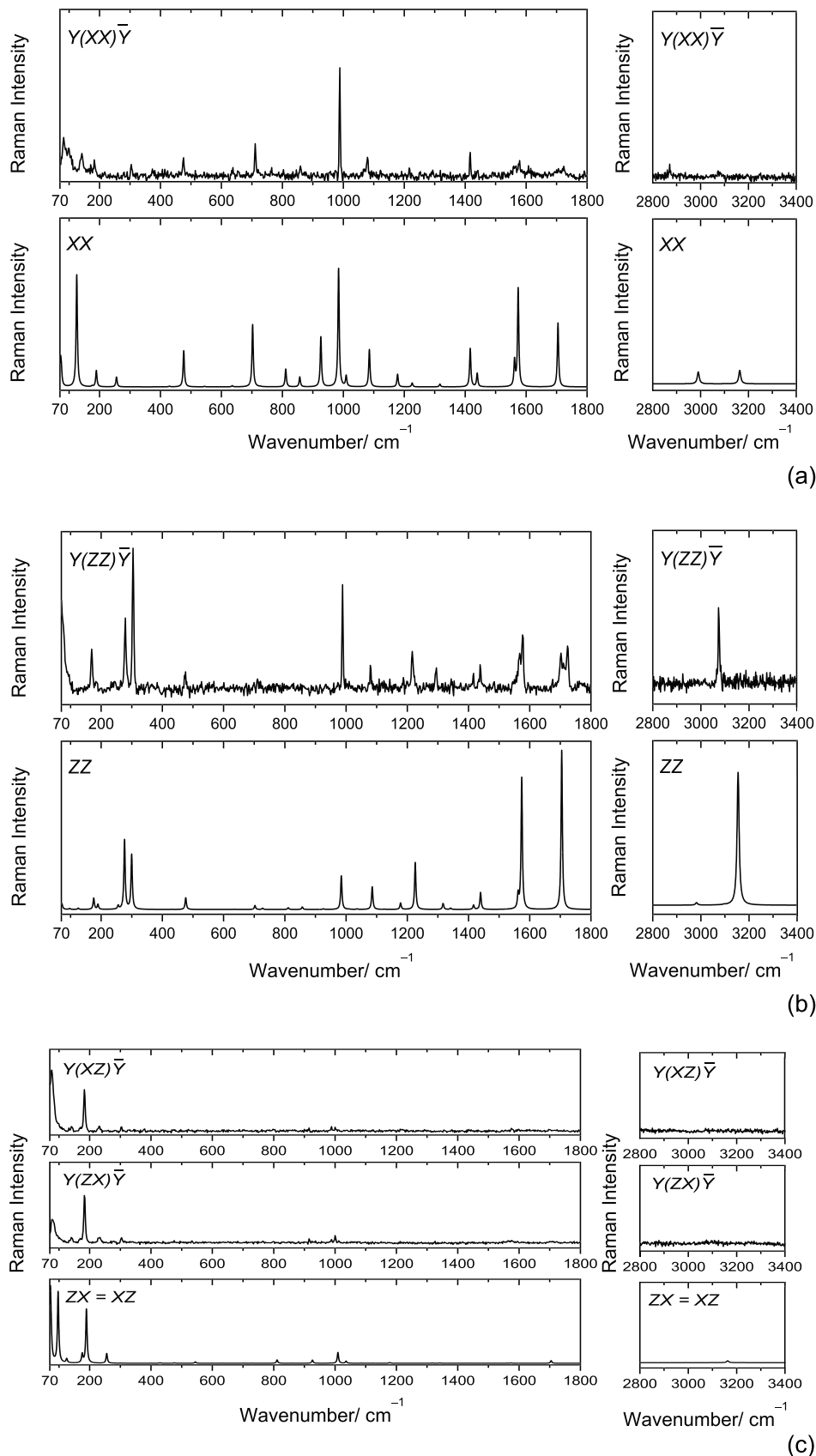


**FIGURE 6** | Experimental polarized  $Y(XX)\bar{Y}$  (VV),  $Y(ZZ)\bar{Y}$  (HH),  $Y(XZ)\bar{Y}$  (VH), and  $Y(ZX)\bar{Y}$  (HV) Raman spectra ( $X$  and  $Z$  are aligned with  $b$  and  $a$  crystallographic axes, respectively) of the BPCA  $P2_1/a$  crystal compared with the B3LYP/pob-TZVP calculated spectra based on the  $ZZ$ ,  $XX$ , and  $ZX=XZ$  component of the crystal Raman tensor. Calculated wavenumbers were scaled by 0.9875.

**TABLE 1** | Calculated Raman wavenumbers ( $\tilde{\nu}/\text{cm}^{-1}$ ), and normalized activities (a) and intensities (I) for the BPCA polycrystalline isotropic Raman spectrum and single crystal polarized spectra, experimentally observed wavenumbers ( $\text{Exp}/\text{cm}^{-1}$ ) and assignments.

Raman No	Sym	Assignment <sup>a</sup>	f	$f_{\text{scal}}^b$	Polycrystalline—Isotropic (iso)										Exp_iso	Single crystal										Exp
					a_iso	I_iso	a_xx	a_yy	a_zz	a_xy	a_xz	a_yz	I_xx	I_yy		I_zz	I_xy	I_xz	I_yz							
155	A <sub>g</sub>	$\nu\text{C(3)-H}$	3233	3164	798.7	783.9	3083	3083	3.1	162.7	535.1	0.0	1.2	0.0	3.1	159.7	525.1	0.0	1.2	0.0	0.0	0.0	0.0	3083		
152	B <sub>g</sub>		3232	3163	148.0	145.3			0.0	0.0	0.0	0.2	0.0	83.7	0.0	0.0	0.0	0.2	0.0	0.0	0.0	0.0	0.0	3082		
151	A <sub>g</sub>	$\nu\text{C(5)-H}$	3232	3163	294.5	289.1	3075	3075	0.0	48.6	211.1	0.0	4.0	0.0	0.0	47.7	207.2	0.0	3.9	0.0	0.0	0.0	0.0	3074		
149	B <sub>g</sub>		3232	3162	160.6	157.7			0.0	0.0	0.0	0.8	0.0	90.3	0.0	0.0	0.0	0.7	0.0	0.0	0.0	0.0	0.0	3074		
147	A <sub>g</sub>	$\nu\text{C(4)-H}$	3173	3105	1000.0	1000.0	3042	3042	0.0	1000.0	2.0	0.0	0.0	0.0	0.0	1000.0	2.0	0.0	0.0	0.0	0.0	0.0	0.0	3042		
145	B <sub>g</sub>		3172	3103	2.5	2.5			0.0	0.0	0.0	0.2	0.0	1.2	0.0	0.0	0.0	0.2	0.0	0.0	0.0	0.0	0.0	3041		
143	B <sub>g</sub>	$\nu\text{C-Hal}$	3057	2992	20.3	21.1	2872	2872	0.0	0.0	0.0	0.7	0.0	10.8	0.0	0.0	0.0	0.8	0.0	0.0	0.0	0.0	0.0	2871		
141	A <sub>g</sub>		3056	2990	392.2	407.2			2.6	348.6	12.5	0.0	0.0	0.0	2.7	362.0	13.0	0.0	0.0	0.0	0.0	0.0	0.0	2871		
139	A <sub>g</sub>	$\nu\text{C=O}$	1742	1705	498.9	908.8	1722/1711/1700	1722/1711/1700	7.8	3.8	453.2	0.0	2.1	0.0	14.2	6.9	825.6	0.0	3.9	0.0	0.0	0.0	0.0	1724/1710/1702		
138	B <sub>g</sub>		1731	1694	33.2	60.8			0.0	0.0	0.0	0.1	0.0	18.8	0.0	0.0	0.0	0.1	0.0	0.0	0.0	0.0	0.0	1722/1697		
136	B <sub>g</sub>	$\nu\text{ring1}$	1609	1574	98.9	195.1	1574/1563	1574/1563	0.0	0.0	0.0	0.2	0.0	55.9	0.0	0.0	0.0	0.3	0.0	0.0	0.0	0.0	0.0	1575		
135	A <sub>g</sub>		1608	1574	368.4	726.7			11.0	6.7	346.1	0.0	0.3	0.0	21.8	13.1	682.7	0.0	0.5	0.0	0.0	0.0	0.0	1577		
132	A <sub>g</sub>	$\nu\text{ring2}$	1596	1562	41.6	82.6	1543	1543	2.8	0.0	36.0	0.0	0.1	0.0	5.6	0.0	71.5	0.0	0.2	0.0	0.0	0.0	0.0	1567		
131	B <sub>g</sub>		1596	1561	35.7	71.0			0.0	0.0	0.0	0.0	0.0	20.3	0.0	0.0	0.0	0.0	0.0	0.0	0.0	0.0	0.0	1565		
128	A <sub>g</sub>	$\delta\text{CH1}; \nu\text{ring4}$	1471	1439	50.4	108.7	1436	1436	1.4	2.8	40.8	0.0	0.1	0.0	3.0	6.0	88.0	0.0	0.1	0.0	0.0	0.0	0.0	1439		
126	B <sub>g</sub>		1469	1437	9.5	20.4			0.0	0.0	0.0	0.0	0.0	5.3	0.0	0.0	0.0	0.1	0.0	0.0	0.0	0.0	0.0	1435		
124	A <sub>g</sub>	$\nu\text{ring5}; \delta\text{CH3}$	1448	1417	54.5	119.5	1414	1414	3.9	31.2	10.2	0.0	0.0	0.0	8.5	68.4	22.4	0.0	0.0	0.0	0.0	0.0	0.0	1416		
121	B <sub>g</sub>		1444	1412	0.1	0.3			0.0	0.0	0.0	0.0	0.0	0.0	0.0	0.0	0.0	0.1	0.0	0.0	0.0	0.0	0.0	Not observed		
119	B <sub>g</sub>	$\delta\text{CH}_{\text{al}}$	1375	1345	14.3	33.1	1352	1352	0.0	0.0	0.0	0.0	0.0	8.1	0.0	0.0	0.0	0.1	0.0	0.0	0.0	0.0	0.0	1354		
117	A <sub>g</sub>		1371	1342	5.7	13.2			0.0	1.9	2.9	0.0	0.2	0.0	0.0	4.4	6.7	0.0	0.5	0.0	0.0	0.0	0.0	1350		
116	A <sub>g</sub>	$\nu\text{ring6}$	1346	1317	33.8	79.6	1291	1291	0.3	14.9	13.6	0.0	0.2	0.0	0.6	35.2	31.9	0.0	0.4	0.0	0.0	0.0	0.0	1294		
113	B <sub>g</sub>		1342	1313	3.7	8.8			0.0	0.0	0.0	0.0	0.0	2.1	0.0	0.0	0.0	0.1	0.0	0.0	0.0	0.0	0.0	1290		
112	A <sub>g</sub>	$\delta\text{CH1}; \nu\text{C-C}$	1253	1226	105.6	267.4	1214	1214	0.3	2.7	96.1	0.0	0.0	0.0	0.9	6.8	243.3	0.0	0.1	0.0	0.0	0.0	0.0	1216		
109	B <sub>g</sub>		1248	1221	11.4	29.1			0.0	0.0	0.0	0.1	0.0	6.4	0.0	0.0	0.0	0.2	0.0	0.0	0.0	0.0	0.0	1212		
108	B <sub>g</sub>	$\delta\text{CH2}$	1205	1179	0.8	2.1	1163	1163	0.0	0.0	0.0	0.0	0.0	0.5	0.0	0.0	0.0	0.0	0.0	0.0	0.0	0.0	0.0	Not observed		
106	A <sub>g</sub>		1204	1178	16.1	42.4			1.1	2.5	12.6	0.0	0.4	0.0	2.8	6.6	33.3	0.0	1.0	0.0	0.0	0.0	0.0	1186		

(Continues)

TABLE 1 | (Continued)

Raman No	Sym	Assignment <sup>a</sup>	f	f <sub>scal</sub> <sup>b</sup>	Polycrystalline—Isotropic (iso)					Single crystal					Exp							
					a <sub>iso</sub>	I <sub>iso</sub>	Exp <sub>iso</sub>	a <sub>xx</sub>	a <sub>yy</sub>	a <sub>zz</sub>	a <sub>xy</sub>	a <sub>xz</sub>	a <sub>yz</sub>	I <sub>xx</sub>		I <sub>yy</sub>	I <sub>zz</sub>	I <sub>xy</sub>	I <sub>xz</sub>	I <sub>yz</sub>		
104	A <sub>g</sub>	$\nu$ ring4	1150	1125	18.3	50.5	1120	0.0	16.8	0.5	0.0	0.1	0.0	0.0	46.3	1.4	0.0	0.1	0.0	0.0	1122	
103	B <sub>g</sub>		1144	1120	0.9	2.4		0.0	0.0	0.0	0.0	0.0	0.5	0.0	0.0	0.0	0.1	0.0	0.0	0.0	1.2	Not observed
100	B <sub>g</sub>	$\delta$ CH3; $\nu$ ring5	1110	1086	0.0	0.1	1078	0.0	0.0	0.0	0.0	0.0	0.0	0.0	0.0	0.0	0.0	0.0	0.0	0.0	0.0	Not observed
98	A <sub>g</sub>		1109	1086	46.7	133.7		2.9	0.1	41.2	0.0	0.1	0.0	8.3	0.4	117.8	0.0	0.3	0.0	0.0	1080	
96	B <sub>g</sub>	$\gamma$ CH2	1061	1038	0.2	0.7	1011	0.0	0.0	0.0	0.1	0.0	0.1	0.0	0.0	0.0	0.2	0.0	0.0	0.2	0.0	Not observed
94	A <sub>g</sub>		1059	1036	2.8	8.3		0.0	0.0	0.9	0.0	1.1	0.0	0.0	0.0	2.7	0.0	0.0	3.2	0.0	1012	
92	B <sub>g</sub>	$\gamma$ CH <sub>al</sub>	1034	1011	5.7	17.6	999	0.0	0.0	0.0	3.2	0.0	0.1	0.0	0.0	0.0	9.8	0.0	0.2	0.0	1001	
90	A <sub>g</sub>		1032	1009	12.2	37.5		0.8	1.2	0.4	0.0	5.2	0.0	2.4	3.7	1.3	0.0	16.1	0.0	0.0	1000	
87	A <sub>g</sub>	$\delta$ ring1	1006	985	147.7	465.7	986	8.3	57.8	55.3	0.0	0.1	0.0	26.2	182.3	174.4	0.0	0.2	0.0	0.0	989	
86	B <sub>g</sub>		1005	984	3.4	10.6		0.0	0.0	0.0	0.1	0.0	1.8	0.0	0.0	0.0	0.3	0.0	0.0	5.7	987	
83	A <sub>g</sub>	$\gamma$ CH3	947	926	6.4	21.4	914	3.3	0.0	1.0	0.0	1.4	0.0	11.1	0.0	3.2	0.0	4.8	0.0	0.0	916	
82	B <sub>g</sub>		946	926	1.3	4.4		0.0	0.0	0.0	0.3	0.0	0.4	0.0	0.0	0.0	1.0	0.0	1.4	0.0	916	
79	A <sub>g</sub>	$\nu$ C-C; $\delta$ ring3	876	857	21.9	79.3	858	0.6	19.1	3.6	0.0	0.0	0.0	2.2	69.1	12.9	0.0	0.1	0.0	0.0	859	
78	B <sub>g</sub>		874	855	0.6	2.1		0.0	0.0	0.0	0.0	0.0	0.3	0.0	0.0	0.0	0.1	0.0	1.1	0.0	858	
75	B <sub>g</sub>	$\gamma$ CH1	832	814	0.2	1.0	795	0.0	0.0	0.0	0.1	0.0	0.0	0.0	0.0	0.0	0.5	0.0	0.0	0.0	828	
74	A <sub>g</sub>		829	811	5.3	20.3		1.0	0.0	2.4	0.0	1.3	0.0	3.9	0.0	9.0	0.0	5.0	0.0	0.0	805	
72	B <sub>g</sub>	$\tau$ ring2	748	732	0.2	0.7	Not observed	0.0	0.0	0.0	0.1	0.0	0.0	0.0	0.0	0.0	0.3	0.0	0.1	0.0	Not observed	
69	A <sub>g</sub>		743	727	1.8	7.6		0.0	0.1	1.5	0.0	0.0	0.0	0.1	0.5	6.5	0.0	0.2	0.0	0.0	Not observed	
68	A <sub>g</sub>	$\delta$ ring3; $\delta$ C=O	718	702	39.2	173.3	708	3.1	25.2	4.6	0.0	0.1	0.0	13.8	111.4	20.5	0.0	0.2	0.0	0.0	711	
67	B <sub>g</sub>		715	700	1.0	4.2		0.0	0.0	0.0	0.0	0.0	0.5	0.0	0.0	0.0	0.0	0.0	2.4	0.0	709	
63	A <sub>g</sub>	$\delta$ ring2	649	636	13.3	65.0	634	0.1	13.1	0.2	0.0	0.0	0.0	0.2	64.1	1.2	0.0	0.1	0.0	0.0	636	
62	B <sub>g</sub>		649	635	0.7	3.4		0.0	0.0	0.0	0.1	0.0	0.3	0.0	0.0	0.0	0.2	0.0	1.7	0.0	634	
60	B <sub>g</sub>	$\gamma$ CBr; $\tau$ ring1	567	555	0.3	1.8	535	0.0	0.0	0.0	0.0	0.0	0.1	0.0	0.0	0.0	0.2	0.0	0.8	0.0	Not observed	
58	A <sub>g</sub>		557	545	0.8	4.8		0.0	0.1	0.1	0.0	0.4	0.0	0.1	0.6	0.5	0.0	2.1	0.0	0.0	533	
56	B <sub>g</sub>	$\delta$ ring3	487	477	9.4	61.1	473	0.0	0.0	0.0	0.0	0.0	5.3	0.0	0.0	0.0	0.3	0.0	34.4	0.0	474	
55	A <sub>g</sub>		487	476	14.4	94.1		1.2	1.5	9.3	0.0	0.1	0.0	8.0	9.8	60.6	0.0	0.6	0.0	0.0	475	

(Continues)

TABLE 1 | (Continued)

Raman	Polycrystalline—Isotropic (iso)										Single crystal										
	No	Sym	Assignment <sup>a</sup>	f	f <sub>scal</sub> <sup>b</sup>	a <sub>iso</sub>	I <sub>iso</sub>	Exp <sub>iso</sub>	a <sub>xx</sub>	a <sub>yy</sub>	a <sub>zz</sub>	a <sub>xy</sub>	a <sub>xz</sub>	a <sub>yz</sub>	I <sub>xx</sub>	I <sub>yy</sub>	I <sub>zz</sub>	I <sub>xy</sub>	I <sub>xz</sub>	I <sub>yz</sub>	Exp
51	B <sub>g</sub>	$\tau$ ring3	444	434	2.8	19.9	422	0.0	0.0	0.0	1.6	0.0	0.0	0.0	0.0	0.0	0.0	11.2	0.0	0.1	423
50	A <sub>g</sub>		439	429	0.3	2.0		0.0	0.0	0.1	0.0	0.1	0.0	0.0	0.1	0.0	0.7	0.0	0.7	0.0	Not observed
48	A <sub>g</sub>	$\nu$ C-Br	306	300	41.4	428.6	301	0.0	9.6	27.3	0.0	0.0	0.0	0.0	0.0	99.8	283.3	0.0	0.2	0.0	304
47	B <sub>g</sub>		305	299	13.9	144.4		0.0	0.0	0.0	0.0	0.0	0.0	7.9	0.0	0.0	0.0	0.1	0.0	81.7	302
44	B <sub>g</sub>	$\delta$ CBr	286	280	0.2	2.8	276	0.0	0.0	0.0	0.1	0.0	0.0	0.0	0.0	0.0	0.0	1.4	0.0	0.1	Not observed
43	A <sub>g</sub>		282	276	33.6	378.0		0.0	0.4	32.0	0.0	0.0	0.0	0.0	0.0	4.7	359.8	0.0	0.1	0.0	279
40	B <sub>g</sub>	$\gamma$ CH <sub>al</sub>	278	272	1.0	11.0	229	0.0	0.0	0.0	0.0	0.0	0.0	0.5	0.0	0.0	0.0	0.2	0.0	5.9	277
38	A <sub>g</sub>		261	256	4.2	50.4		0.2	0.5	1.5	0.0	1.2	0.0	0.0	2.2	6.1	18.5	0.0	14.5	0.0	233
35	B <sub>g</sub>	$\tau$ ring1	203	199	0.4	7.0	181	0.0	0.0	0.0	0.2	0.0	0.0	0.0	0.0	0.0	0.0	3.6	0.0	0.5	188
34	A <sub>g</sub>		194	189	10.9	178.0		0.2	0.6	1.6	0.0	4.9	0.0	0.0	3.6	10.0	25.9	0.0	80.1	0.0	183
32	B <sub>g</sub>	wCHO; $\tau$ C-C	184	180	3.1	52.9	167	0.0	0.0	0.0	1.3	0.0	0.4	0.0	0.0	0.0	0.0	22.9	0.0	7.1	181
31	A <sub>g</sub>		180	176	7.6	133.8		0.0	3.8	3.3	0.0	0.7	0.0	0.2	0.2	67.0	58.5	0.0	12.9	0.0	170
29	B <sub>g</sub>	$\tau$ C-C	174	170	6.8	125.1	167	0.0	0.0	0.0	3.4	0.0	0.5	0.0	0.0	0.0	0.0	62.3	0.0	8.8	167
25	B <sub>g</sub>	InterMol	130	127	2.6	62.5	138	0.0	0.0	0.0	0.8	0.0	0.6	0.0	0.0	0.0	0.0	20.3	0.0	15.2	140
24	A <sub>g</sub>	$\tau$ C-C	128	125	1.8	45.4	138	1.0	0.4	0.3	0.0	0.2	0.0	24.8	8.7	6.4	6.4	0.0	6.0	0.0	140
22	B <sub>g</sub>	InterMol	103	100	7.2	221.3	95	0.0	0.0	0.0	4.1	0.0	0.0	0.0	0.0	0.0	0.0	125.5	0.0	0.0	98
20	A <sub>g</sub>	InterMol	99	97	6.0	192.7	95	0.0	0.1	0.2	0.0	3.3	0.0	0.0	0.0	2.2	4.8	0.0	104.8	0.0	98
18	B <sub>g</sub>	InterMol	89	87	2.7	97.2	95	0.0	0.0	0.0	0.1	0.0	1.5	0.0	0.0	0.0	0.0	2.1	0.0	52.9	82
17	A <sub>g</sub>	InterMol	76	75	1.3	55.8	79	0.1	0.5	0.0	0.0	0.5	0.0	2.9	20.4	0.4	0.4	0.0	19.6	0.0	79
15	A <sub>g</sub>	InterMol	74	72	4.4	189.3	79	0.1	0.1	0.4	0.0	2.1	0.0	4.7	2.2	19.0	0.0	0.0	92.3	0.0	77
14	B <sub>g</sub>	InterMol	72	71	11.8	516.3	79	0.0	0.0	0.0	6.6	0.0	0.1	0.0	0.0	0.0	0.0	289.7	0.0	3.1	80
12	A <sub>g</sub>	InterMol	68	67	3.6	164.9		0.1	0.0	1.2	0.0	1.3	0.0	3.7	0.5	54.8	0.0	62.2	0.0	0.0	
8	B <sub>g</sub>	InterMol	47	46	0.5	34.2		0.0	0.0	0.0	0.0	0.0	0.3	0.0	0.0	0.0	0.0	0.0	0.0	19.5	
7	A <sub>g</sub>	InterMol	42	41	0.4	33.8		0.0	0.2	0.0	0.0	0.1	0.0	0.0	0.0	14.3	1.5	0.0	9.0	0.0	
6	B <sub>g</sub>	InterMol	38	38	0.3	24.0		0.0	0.0	0.0	0.1	0.0	0.1	0.0	0.0	0.0	0.0	8.3	0.0	5.0	
4	A <sub>g</sub>	InterMol	24	23	2.7	360.7		0.0	0.0	0.0	0.0	1.5	0.0	5.4	0.0	0.0	0.0	201.1	0.0	0.0	

<sup>a</sup>The mode designations follow the notation used in ref. [1];  $\nu$ , stretching;  $\delta$ , in-plane bending;  $\gamma$ , out-of-plane rocking; w, wagging;  $\tau$ , torsion; al, aldehyde; InterMol, intermolecular mode.

<sup>b</sup>Scaled calculated wavenumbers (by 0.9875).

**TABLE 2** | Calculated infrared wavenumbers ( $f/\text{cm}^{-1}$ ) and intensities ( $I/\text{kmol}^{-1}$ ), experimentally observed wavenumbers ( $\text{Exp}/\text{cm}^{-1}$ ) and assignments.

Infrared						
No	Sym	Assignment <sup>a</sup>	f	$f_{\text{scal}}^b$	I	Exp
156	B <sub>u</sub>	$\nu\text{C(3)-H}$	3234	3165	152.6	3081
<b>154</b>	<b>A<sub>u</sub></b>		<b>3233</b>	<b>3163</b>	<b>69.9</b>	
153	B <sub>u</sub>	$\nu\text{C(5)-H}$	3232	3163	72.6	3074
<b>150</b>	<b>A<sub>u</sub></b>		<b>3232</b>	<b>3162</b>	<b>20.5</b>	
148	B <sub>u</sub>	$\nu\text{C(4)-H}$	3173	3105	0.1	3039
<b>146</b>	<b>A<sub>u</sub></b>		<b>3172</b>	<b>3103</b>	<b>379.8</b>	
<b>144</b>	<b>A<sub>u</sub></b>	$\nu\text{C-Hal}$	<b>3058</b>	<b>2992</b>	<b>132.0</b>	2871/2846
142	B <sub>u</sub>		3056	2991	1.4	
140	B <sub>u</sub>	$\nu\text{C=O}$	1755	1717	1824.1	1726/1712/1701
<b>137</b>	<b>A<sub>u</sub></b>		<b>1730</b>	<b>1692</b>	<b>1.5</b>	
134	B <sub>u</sub>	$\nu\text{ring1}$	1608	1573	98.1	1572
<b>133</b>	<b>A<sub>u</sub></b>		<b>1607</b>	<b>1573</b>	<b>94.8</b>	
<b>130</b>	<b>A<sub>u</sub></b>	$\nu\text{ring2}$	<b>1595</b>	<b>1561</b>	<b>132.9</b>	1553/1542
129	B <sub>u</sub>		1594	1560	310.3	
<b>127</b>	<b>A<sub>u</sub></b>	$\delta\text{CH1}; \nu\text{ring4}$	<b>1469</b>	<b>1437</b>	<b>172.5</b>	1434
125	B <sub>u</sub>		1469	1437	297.4	
123	B <sub>u</sub>	$\nu\text{ring5}; \delta\text{CH3}$	1447	1415	82.0	1413
<b>122</b>	<b>A<sub>u</sub></b>		<b>1445</b>	<b>1414</b>	<b>107.9</b>	
120	B <sub>u</sub>	$\delta\text{CHal}$	1377	1348	7.4	1351
<b>118</b>	<b>A<sub>u</sub></b>		<b>1372</b>	<b>1343</b>	<b>45.9</b>	
115	B <sub>u</sub>	$\nu\text{ring6}$	1345	1316	212.1	1289
<b>114</b>	<b>A<sub>u</sub></b>		<b>1342</b>	<b>1313</b>	<b>27.8</b>	
111	B <sub>u</sub>	$\delta\text{CH1}; \nu\text{C-C}$	1250	1223	246.3	1214
<b>110</b>	<b>A<sub>u</sub></b>		<b>1249</b>	<b>1222</b>	<b>148.0</b>	
107	B <sub>u</sub>	$\delta\text{CH2}$	1204	1179	8.5	1163
<b>105</b>	<b>A<sub>u</sub></b>		<b>1203</b>	<b>1178</b>	<b>0.1</b>	
102	B <sub>u</sub>	$\nu\text{ring4}$	1144	1119	815.2	1116
<b>101</b>	<b>A<sub>u</sub></b>		<b>1142</b>	<b>1117</b>	<b>32.1</b>	
99	B <sub>u</sub>	$\delta\text{CH3}; \nu\text{ring5}$	1109	1086	0.7	1078
<b>97</b>	<b>A<sub>u</sub></b>		<b>1108</b>	<b>1085</b>	<b>20.3</b>	
<b>95</b>	<b>A<sub>u</sub></b>	$\gamma\text{CH2}$	<b>1059</b>	<b>1037</b>	<b>1.0</b>	1013
93	B <sub>u</sub>		1059	1036	0.6	
<b>91</b>	<b>A<sub>u</sub></b>	$\gamma\text{CHal}$	<b>1033</b>	<b>1010</b>	<b>0.0</b>	998
89	B <sub>u</sub>		1029	1007	11.1	
88	B <sub>u</sub>	$\delta\text{ring1}$	1008	986	5.4	985
<b>85</b>	<b>A<sub>u</sub></b>		<b>1005</b>	<b>983</b>	<b>144.6</b>	

(Continues)

TABLE 2 | (Continued)

Infrared						
No	Sym	Assignment <sup>a</sup>	f	f <sub>scal</sub> <sup>b</sup>	I	Exp
<b>84</b>	<b>A<sub>u</sub></b>	<b>γCH3</b>	<b>948</b>	<b>928</b>	<b>1.3</b>	914
81	B <sub>u</sub>		945	925	10.1	
80	B <sub>u</sub>	<b>νC-C; δring3</b>	876	857	12.1	854
<b>77</b>	<b>A<sub>u</sub></b>		<b>871</b>	<b>852</b>	<b>232.0</b>	
<b>76</b>	<b>A<sub>u</sub></b>	<b>γCH1</b>	<b>834</b>	<b>816</b>	<b>10.9</b>	794
73	B <sub>u</sub>		827	809	298.1	
<b>71</b>	<b>A<sub>u</sub></b>	<b>τring2</b>	<b>746</b>	<b>730</b>	<b>1.2</b>	716
70	B <sub>u</sub>		743	727	34.7	
66	B <sub>u</sub>	<b>δring3; δC=O</b>	713	698	425.1	706
<b>65</b>	<b>A<sub>u</sub></b>		<b>712</b>	<b>697</b>	<b>0.0</b>	
64	B <sub>u</sub>	<b>δring2</b>	651	637	80.2	632
<b>61</b>	<b>A<sub>u</sub></b>		<b>647</b>	<b>633</b>	<b>209.8</b>	
<b>59</b>	<b>A<sub>u</sub></b>	<b>γCBr; τring1</b>	<b>561</b>	<b>548</b>	<b>0.0</b>	555
57	B <sub>u</sub>		555	543	0.9	
54	B <sub>u</sub>	<b>δring3</b>	486	476	10.0	471
<b>53</b>	<b>A<sub>u</sub></b>		<b>484</b>	<b>474</b>	<b>10.8</b>	
<b>52</b>	<b>A<sub>u</sub></b>	<b>τring3</b>	<b>444</b>	<b>434</b>	<b>0.0</b>	417
49	B <sub>u</sub>		438	429	19.5	
46	B <sub>u</sub>	<b>νC-Br</b>	304	298	75.2	
<b>45</b>	<b>A<sub>u</sub></b>		<b>303</b>	<b>296</b>	<b>1.5</b>	
42	B <sub>u</sub>	<b>δCBr</b>	281	275	19.2	
<b>41</b>	<b>A<sub>u</sub></b>		<b>280</b>	<b>274</b>	<b>33.8</b>	
<b>39</b>	<b>A<sub>u</sub></b>	<b>γCHal</b>	<b>270</b>	<b>265</b>	<b>0.5</b>	
37	B <sub>u</sub>		251	246	154.3	
<b>36</b>	<b>A<sub>u</sub></b>	<b>τring1</b>	<b>203</b>	<b>199</b>	<b>0.3</b>	
33	B <sub>u</sub>		190	186	12.4	
<b>30</b>	<b>A<sub>u</sub></b>	<b>wCHO; τC-C</b>	<b>177</b>	<b>173</b>	<b>16.8</b>	
28	B <sub>u</sub>		172	168	7.1	
<b>27</b>	<b>A<sub>u</sub></b>	<b>τC-C</b>	<b>168</b>	<b>164</b>	<b>19.9</b>	
26	B <sub>u</sub>		135	132	24.2	
<b>23</b>	<b>A<sub>u</sub></b>	<b>InterMol</b>	<b>124</b>	<b>122</b>	<b>0.0</b>	
<b>21</b>	<b>A<sub>u</sub></b>	<b>InterMol</b>	<b>101</b>	<b>99</b>	<b>0.2</b>	
19	B <sub>u</sub>	<b>InterMol</b>	94	92	35.2	
16	B <sub>u</sub>	<b>InterMol</b>	74	73	6.8	
<b>13</b>	<b>A<sub>u</sub></b>	<b>InterMol</b>	<b>72</b>	<b>71</b>	<b>0.6</b>	
<b>11</b>	<b>A<sub>u</sub></b>	<b>InterMol</b>	<b>59</b>	<b>57</b>	<b>0.3</b>	
<b>10</b>	<b>A<sub>u</sub></b>	<b>InterMol</b>	<b>53</b>	<b>52</b>	<b>1.0</b>	

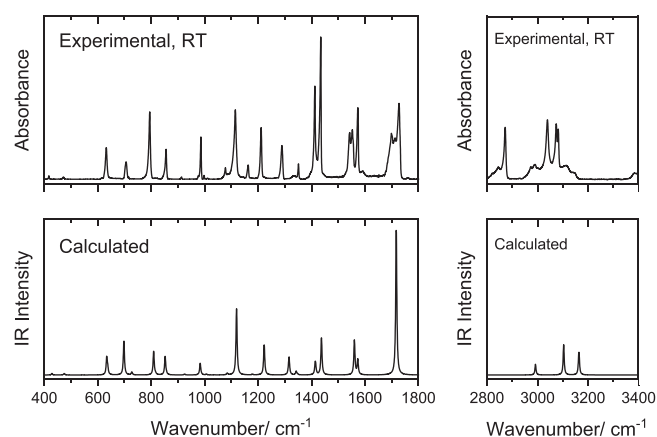
(Continues)

TABLE 2 | (Continued)

Infrared						
No	Sym	Assignment <sup>a</sup>	f	f <sub>scal</sub> <sup>b</sup>	I	Exp
9	B <sub>u</sub>	InterMol	49	48	0.6	
5	B <sub>u</sub>	InterMol	25	25	0.6	
3	B <sub>u</sub>	Acoustic (T <sub>x</sub> )	0	0	0.0	
2	A <sub>u</sub>	Acoustic (T <sub>y</sub> )	0	0	0.0	
1	B <sub>u</sub>	Acoustic (T <sub>z</sub> )	0	0	0.0	

<sup>a</sup>The mode designations follow the notation used in ref. [1];  $\nu$ , stretching;  $\delta$ , in-plane bending;  $\gamma$ , out-of-plane rocking; w, wagging;  $\tau$ , torsion; al, aldehyde; InterMol, intermolecular mode.

<sup>b</sup>Scaled calculated wavenumbers (by 0.9875).



**FIGURE 7** | Experimental room-temperature ATR-IR spectrum of the polycrystalline BPCA compared with the BPCA P2<sub>1</sub>/a crystal B3LYP/pob-TZVP calculated infrared spectrum. Calculated wavenumbers were scaled by 0.9875.

the reassignment of the out-of-plane rocking mode of the aldehyde fragment ( $\gamma\text{CH}_{\text{al}}$ ) and that of the  $\gamma\text{CH}_2$  mode the opposite way when compared with the previously suggested assignments [1], with the first mode assigned to a band observed at a slightly higher wavenumber than that assigned to the last vibration. All other assignments now made based on the fully periodic crystal calculations agree with those previously made based on the spectra of the isolated molecule of the compound [1].

## 4 | Conclusion

Polarized Raman spectra of single crystals of BPCA were measured at RT and analyzed with the support of fully periodic DFT calculations for its monoclinic crystal structure (space group P2<sub>1</sub>/a, No. 14). These computations, carried out using the CRYSTAL software with the B3LYP hybrid functional and the polarization-consistent pob-TZVP basis set, demonstrated excellent agreement with the experimental spectra. This enabled a precise assignment of the A<sub>g</sub> and B<sub>g</sub> Raman-active modes to specific spectral bands. Additionally, the isotropic (non-polarized) Raman spectrum of BPCA was simulated and likewise matched the experimental data closely. The room-temperature IR spectrum of BPCA was also re-examined in light of the periodic

calculations, providing a more accurate interpretation than earlier studies based on molecular (non-crystalline) models. In the studied crystalline system, intermolecular interactions exert only a minor influence on the intramolecular vibrational potential. As such, this study also served as a benchmark for the employed computational approach, demonstrating its ability to capture well the effects of both crystallographic periodicity and symmetry on the polarization features of vibrational spectra.

## Author Contributions

**Anna Luiza B. Brito:** experimental planning, experiments, spectroscopic data analysis, writing of the preliminary version of the manuscript. **Bernardo A. Nogueira:** experimental planning, experiments, spectroscopic data analysis, writing of the preliminary version of the manuscript. **Gulce O. Ildiz:** spectroscopic data analysis, funding acquisition. **Rui Fausto:** conceptualization, experiments planning, data analysis, writing of the preliminary version of the manuscript, funding acquisition. All authors contributed to the final written version of the manuscript.

## Acknowledgments

This study has also been supported by the European Research Agency (European Union) through the Horizon-Widera-2023-Talents-01 ERA-Chair 1011848998: Spectroscopy@IKU “Manipulating and Characterizing Molecular Architectures: From Isolated Molecules to Molecular Crystals.” The CQC-IMS is supported by FCT through projects UI0313B/QUI/2025, UI0313P/QUI/2025 and LA/P/0056/2020. The authors also acknowledge the Laboratory for Advanced Computing at University of Coimbra (LCA-UC; <https://www.uc.pt/lca>) for providing computing resources.

## Conflicts of Interest

The authors declare no conflicts of interest.

## Data Availability Statement

The data that support the findings of this study are available from the corresponding author upon reasonable request.

## References

1. A. L. B. Brito, S. Lopes, G. O. Ildiz, and R. Fausto, “Structure, Vibrational Spectra, and Cryogenic MatrixPhotochemistry of 6-Bromopyridine-2-carbaldehyde: From the Single Molecule of the Compound to the Neat Crystalline Material,” *Molecules* 28 (2023): 1673.
2. X. Li, C. L. D. Gibb, M. E. Kuebel, and B. C. Gibb, “Two New Ligands for Carbonic Anhydrase Mimicry,” *Tetrahedron* 57 (2001): 1175–1182.

3. A. Orita, T. Nakano, T. Yokoyama, G. Babu, and J. Otera, "Double Elimination Protocol for Access to Pyridine-Containing Arylene-Ethylenes," *Chemistry Letters* 33, no. 10 (2004): 1298–1299.
4. M. Tanaka and R. J. Young, "Review Polarised Raman Spectroscopy for the Study of Molecular Orientation Distributions in Polymers," *Journal of Materials Science* 41 (2006): 963–991.
5. J. Baran, M. Drozd, T. Gavrilko, and M. Trzebiatowska, "The Analysis of Sarcosine Phosphate Single Crystal Based on Polarized IR and Raman Spectra," *Journal of Molecular Structure* 1319, no. Part 2 (2025): 139635.
6. V. V. Poborchii, "Oriented Se<sub>6</sub> Ring Clusters in Zeolite Single Crystals: Polarized Raman Microscopy, Optical Absorption Spectra and Photo-Induced Effects," *Microporous and Mesoporous Materials* 308 (2020): 110559.
7. T. Onuma, S. Fujioka, T. Yamaguchi, et al., "Polarized Raman Spectra in  $\beta$ -Ga<sub>2</sub>O<sub>3</sub> Single Crystals," *Journal of Crystal Growth* 401 (2014): 330–333.
8. B. A. Nogueira, S. M. M. Lopes, T. M. V. D. Pinho e Melo, et al., "Molecular and Crystal Structures of *N*-picryl-*m*-phenolidine and Investigation of Single Crystal Polarized Raman Spectra," *Journal of Molecular Structure* 1262 (2022): 133111.
9. S. K. Srivastava and P. K. Kushwaha, eds., *Raman Spectroscopy* (Springer Series in Optical Sciences, 2024): 101–122.
10. D. Wiebolt, R. Heintz, M. Wall, "Thermo Scientific Application Note 2016; 52792".
11. B. A. Nogueira, A. Milani, C. Castiglioni, and R. Fausto, "The Correlation Between Experimental Polarized Raman Spectra and Their Density Functional Theory Prediction in the LCAO Framework: The R3c LiNbO<sub>3</sub> Crystal as a Test Case," *Journal of Raman Spectroscopy* 52, no. 5 (2021): 995–1010.
12. B. A. Nogueira, M. Rérat, R. Fausto, C. Castiglioni, and R. Dovesi, "Raman Activity of the Longitudinal Optical Phonons of the LiNbO<sub>3</sub> Crystal: Experimental Determination and Quantum Mechanical Simulation," *Journal of Raman Spectroscopy* 53, no. 11 (2022): 1904–1914.
13. G. Keresztury, *Handbook of Vibrational Spectroscopy*, ed. J. M. Chalmers (John Wiley & Sons, Ltd., 2006).
14. R. Loudon, "The Raman Effect in Crystals," *Advances in Physics* 13, no. 52 (1964): 423–482.
15. G. Turrell, *Infrared and Raman Spectra of Crystals* (Academic Press, 1972).
16. J. C. Decius and R. M. Hexter, *Molecular Vibrations in Crystals* (McGraw-Hill, 1977).
17. J. Kim, J. U. Lee, and H. Cheong, "Polarized Raman Spectroscopy for Studying Two-Dimensional Materials," *Journal of Physics: Condensed Matter* 32 (2020): 343001.
18. R. Dovesi, A. Erba, R. Orlando, et al., "Quantum-Mechanical Condensed Matter Simulations With CRYSTAL," *Wiley Interdisciplinary Reviews: Computational Molecular Science* 8, no. 4 (2018): e1360.
19. H.-X. Zhang, D.-B. Qin, L.-H. Jing, S.-J. Gu, and Z.-H. Mao, "6-Bromopyridine-2-carbaldehyde," *Acta Crystallographica Section E: Crystallographic Data Communications* 62 (2006): 1715–1716.
20. C. Lee, W. Yang, and R. G. Parr, "Development of the Colle-Salvetti Correlation-Energy Formula Into a Functional of the Electron Density," *Physical Review B* 37 (1988): 785–789.
21. J. Laun, D. V. Oliveira, and T. Bredow, "Consistent Gaussian Basis Sets of Double- and Triple-Zeta Valence With Polarization Quality of the Fifth Period for Solid-State Calculations," *Journal of Computational Chemistry* 39, no. 19 (2018): 1285–1290.
22. R. Dovesi, R. Orlando, A. Erba, et al., "CRYSTAL14: A Program for the *Ab Initio* Investigation of Crystalline Solids," *International Journal of Quantum Chemistry* 114, no. 19 (2014): 1287–1317.
23. B. Montanari, B. Civalleri, C. M. Zicovich-Wilson, and R. Dovesi, "Influence of the Exchange-Correlation Functional in All-Electron Calculations of the Vibrational Frequencies of Corundum ( $\alpha$ -Al<sub>2</sub>O<sub>3</sub>)," *International Journal of Quantum Chemistry* 106, no. 7 (2006): 1703–1714.
24. F. Pascale, M. Catti, A. Damin, R. Orlando, V. R. Saunders, and R. Dovesi, "Vibration Frequencies of Ca<sub>3</sub>Fe<sub>2</sub>Si<sub>3</sub>O<sub>12</sub> Andradite: An *Ab Initio* Study With the CRYSTAL Code," *Journal of Physical Chemistry B* 109, no. 39 (2005): 18522–18527.
25. F. Pascale, C. M. Zicovich-Wilson, F. López Gejo, B. Civalleri, R. Orlando, and R. Dovesi, "The Calculation of the Vibrational Frequencies of Crystalline Compounds and Its Implementation in the CRYSTAL Code," *Journal of Computational Chemistry* 25, no. 6 (2004): 888–897.
26. C. M. Zicovich-Wilson, F. Pascale, C. Roetti, V. R. Saunders, R. Orlando, and R. Dovesi, "Calculation of the Vibration Frequencies of  $\alpha$ -Quartz: The Effect of Hamiltonian and Basis Set," *Journal of Computational Chemistry* 25, no. 15 (2004): 1873–1881.